Supporting Information

Observation and Kinetic Characterization of Transient Schiff Base Intermediates by CEST NMR Spectroscopy

Venkatraman Ramanujam[+], Cyril Charlier[+],* and Ad Bax*

anie_201908416_sm_miscellaneous_information.pdf

Dicatechol pyrrole dialanine (DCPdA) purification and characterization by NMR: DCPdA adduct purification was carried out on a Waters 2545 HPLC system. DCPdA was purified from a 6 ml reaction containing 2 mM DOPAL and 10 mM dialanine in 10 mM sodium phosphate buffer pH 7.5 after incubation at 310 K for 3 hours. A C18 column with the following dimensions was used 2.1 x 50 mm, 3.5 µm particle size (Agilent #885750-902). The column was equilibrated with buffer A (water and 0.05% trifluoroacetic acid) at a flowrate of 0.5 ml/min. After loading the sample, the column was washed with 10 column volumes of buffer A and then a gradient of acetonitrile was developed from 0 to 30% at 0.5%/min. Fractions containing DCPdA were pooled, flash frozen with liquid nitrogen, and lyophilized in the dark. NMR samples were prepared by resuspending the product in deuterated methanol (Sigma-Aldrich). Samples of dialanine and DOPAL used to measure chemical shifts in Table S1 were also prepared in deuterated methanol. NMR data were collected for the DCPdA, dialanine, and DOPAL samples at 298 K on a 600 MHz Bruker spectrometer equipped with a z-axis cryogenic probe. The reported chemical shifts were measured from ^{1}H-^{13}C HSQC and ^{1}H-^{13}C HMBC spectra and ^{1}H and ^{13}C chemical shifts were referenced to the methanol solvent signal at 3.31 and 49.15 ppm, respectively.

NMR Sample Preparation and Data collection
3,4-Dihydroxyphenylacetaldehyde (DOPAL) (VDM Biochemicals) was dissolved in deuterated methanol (Sigma--Aldrich) at a concentration of 300 mM. The prepared DOPAL stocks were aliquoted and stored at -80 °C. For NMR measurements, the DOPAL stock was then diluted to a concentration of 2 mM in 10 mM sodium phosphate dissolved in D_2O, pD 7.9. The sample was deoxygenated by sparging nitrogen gas through the sample for 3 h. The sample was subsequently equilibrated for 8 h at 37 °C to allow for complete exchange of the DOPAL methylene protons with deuterons, prior to recording of NMR spectra. For the reactions of DOPAL with A_2 and AcL, either 10 mM A_2 (Sigma--Aldrich) or 30 mM N^α-acetyl lysine (Sigma--Aldrich) was added to the deuterium exchanged DOPAL solution, which was again deoxygenated by sparging with nitrogen before NMR data acquisition.

 All NMR measurements were carried out at 600 MHz on a Bruker Avance spectrometer equipped with a cryogenic probe and pulsed field gradients. Three samples each contained 2mM DOPAL in the absence or presence of either 10 mM A_2 or 30 mM Nα-acetyl lysine dissolved in 10 mM $NaDPO_4$-D_2O buffer (pD 7.9). All CEST spectra were acquired following an initial continuous CEST saturation pulse terminated by a short (1 ms) pulsed field gradient to eliminate any residual transverse water signal prior to a 90º observe pulse, followed by signal detection. Due to the long T_1 of the aldehyde ^{1}H in the deoxygenated, methylene-deuterated DOPAL sample ($T_1 \approx 25$ s) a long interscan delay of 60 s was used. For signals not directly observable in the 1D spectrum, a CEST profile varying the irradiation frequency was recorded to determine their resonance frequency. The intensity saturation profile as a function of CEST ^{1}H frequency contained at least five points and was fitted to a second order polynomial function to obtain the center of the resonance. Once the resonance frequency was known for each state, saturation profiles of the aldehyde signal were recorded by irradiating one of the minor states on-resonance as a function of saturation time, τ_{cest}, and saturation field, B_1. For all experiments, reference points (I_0) were recorded at the start and end of the series, with either the saturation time $\tau_{cest} = 0$ s or saturation field $B_1 = 0$ Hz. All saturation profiles shown correspond to the ratio of the spectra with and without saturation (I/I_0). All NMR spectra were processed using nmrPipe.[1]

^{1}H-CEST Data Analysis

Spectral intensities were obtained using an in-house python script based on the nmrglue program.[2] All the CEST intensity profiles were analyzed using an in-house-written python program, accessible through https://github.com/ XYZ, which minimizes the root-mean-square difference (rmsd) given by:

$$rmsd(\theta) = \sum_{i=1}^{N} \left(I_i^{exp} - I_i^{sim}(\theta) \right)^2 \tag{S1}$$

where I_i^{exp} refers to the experimental normalized intensity, I_i^{sim} is the simulated normalized intensity and θ represents the different fitting parameters. Errors of I_i^{exp} include both the thermal noise as well as the effects of small drifts in spectrometer settings and slow degradation of the sample, in particular at higher temperatures. The effective size of these errors were estimated automatically using a 1000-step Bootstrap (case resampling) simulation.[3] To account for B_1 inhomogeneity, each trajectory was calculated as a weighted sum of 10 simulations with B_1 fields evenly spaced between $\pm 2\sigma$ around the nominal field strength, where σ is the standard deviation of the B_1 field distribution, estimated at 10%.[4]

Fitting of ^{1}H-CEST data on DOPAL equilibrium

The simulated intensities for ^{1}H-CEST attenuation profiles (I/I_0) for DOPAL in the absence of dialanine/Nα-acetyl lysine were obtained using the homogeneous form of the Bloch-McConnell equations for a single spin in a two-site exchange model between the sites A (gem-diol) and B (aldehyde):

$$\frac{d}{dt}\begin{pmatrix} E \\ I_x^A \\ I_y^A \\ I_z^A \\ I_x^B \\ I_y^B \\ I_z^B \end{pmatrix} = \begin{pmatrix} 0 & 0 & 0 & 0 & 0 & 0 & 0 \\ 0 & -R_2^A - k_{AB} & -\omega_A & \omega_1 & k_{BA} & 0 & 0 \\ 0 & \omega_a & -R_2^A - k_{AB} & 0 & 0 & k_{BA} & 0 \\ 2I_{eq}^A R_1^A & -\omega_1 & 0 & -R_1^A - k_{AB} & 0 & 0 & k_{BA} \\ 0 & k_{AB} & 0 & 0 & -R_2^B - k_{BA} & -\omega_B & \omega_1 \\ 0 & 0 & k_{AB} & 0 & \omega_B & -R_2^B - k_{BA} & 0 \\ 2I_{eq}^B R_1^B & 0 & 0 & k_{AB} & -\omega_1 & 0 & -R_1^B - k_{AB} \end{pmatrix} \begin{pmatrix} E \\ I_x^A \\ I_y^A \\ I_z^A \\ I_x^B \\ I_y^B \\ I_z^B \end{pmatrix}$$

$$\tag{S2}$$

Where $I_x^A, I_y^A, \dots$ represent the magnetization components of each spin, k_{AB} and k_{BA} are respectively the aldehyde hydration and dehydration rate constants, $R_1^{A,B} = (1/T_1^{A,B})$, and $R_2^{A,B} = (1/T_2^{A,B})$ are the longitudinal and transverse relaxation rates. $\omega_{A,B}$ are the angular resonance frequencies, ω_1 is the strength of the saturation RF field in units of rad/s. I_{eq}^A and I_{eq}^B are the equilibrium populations of states A and B. Here, $\omega_{A,B}$ were experimentally determined (Figure S2). For the DOPAL hydration equilibrium, the ratio of the equilibrium populations was derived from the integrals of the gem-diol and aldehyde resonances by integration of the 1D spectrum at each temperature, making k_{ex} to be the only fitting parameter, with $k_{AB} = p_B k_{ex}$ and $k_{BA} = p_A k_{ex}$. T$_1$ was measured at ~25 s but showed *ca* 10% sample by sample variation, depending on the completeness of deoxygenation. T$_2$, which is impacted by unresolved scalar coupling to the rapidly relaxing α-methylene deuterons, was set to 1 s for both states. Uncertainty in this T$_2$ value does not significantly impact the saturation profile (Figure S8).

Fitting ¹H-CEST data of DOPAL-A₂ and DOPAL-AcL equilibria

The modeling of these equilibria is described by the four-state kinetic scheme shown below, where A is the gem-diol, B is the aldehyde, C is the hemiaminal (hydrated Schiff base) and D is the Schiff base.

$$
\begin{array}{ccccccc}
 & k_{AB} & & k_{BC} & & k_{CD} & \\
A & \rightleftharpoons & B & \rightleftharpoons & C & \rightleftharpoons & D \\
 & k_{BA} & & k_{CB} & & k_{DC} &
\end{array}
\tag{S3}
$$

As the equilibrium reaction between gem-diol and aldehyde is not significantly perturbed by the addition of A₂ or AcL, the rate constants k_{AB} and k_{BA} were fixed to values obtained from the DOPAL hydration equilibrium fitting (Figure S1). For the reaction with A₂, the direct observation of the Schiff base (DSB$_{A2}$) resonance allowed us to fix the ratio $\frac{p_D}{p_B} = 4\%$ at all temperatures. This additional constraint reduced the number of fitting parameters to only 3: k_{BC}, k_{CB}, and k_{CD}. k_{DC} was then calculated from the relationship $k_{DC} = (k_{CD}k_{BC})/(k_{CB}p_D/p_B)$. For the reaction with AcL, all 4 rates (k_{BC}, k_{CB}, k_{CD} and k_{DC}) were optimized at each temperature. The populations of each state were then determined *a posteriori* from the exchange rates:

$$
\begin{Bmatrix} p_A \\ p_B \\ p_C \\ p_D \end{Bmatrix} = \begin{Bmatrix} \dfrac{1}{1+\frac{k_{AB}}{k_{BA}}\left[1+\frac{k_{BC}}{k_{CB}}\left(1+\frac{k_{CD}}{k_{DC}}\right)\right]} \\[2ex] \dfrac{p_A k_{AB}}{k_{BA}} \\[2ex] \dfrac{p_A k_{AB} k_{BC}}{k_{BA} k_{CB}} \\[1ex] 1 - p_A - p_B - p_C \end{Bmatrix}
\tag{S4}
$$

The saturation curves (I/I_0), were calculated using the Bloch-McConnell equation for the four-state model using Equation S5, where R_1^n (25 s) and R_2^n (1 s) are the longitudinal and transverse relaxation rates for state n (all assumed to have the same value), ω_n is the angular chemical shifts of state n, and k_{AB} k_{BA}, k_{BC}, k_{CB}, k_{CD} and k_{DC} are the exchange rates.

$$
\frac{d}{dt}
\begin{bmatrix}
E/2 \\ I_x^A \\ I_y^A \\ I_z^A \\ I_x^B \\ I_y^B \\ I_z^B \\ I_x^C \\ I_y^C \\ I_z^C \\ I_x^D \\ I_y^D \\ I_z^D
\end{bmatrix}
= -
\begin{bmatrix}
0 & 0 & 0 & 0 & 0 & 0 & 0 & 0 & 0 & 0 & 0 & 0 & 0 \\
0 & R_2^A+k_{AB} & \omega_A & 0 & -k_{BA} & 0 & 0 & 0 & 0 & 0 & 0 & 0 & 0 \\
0 & -\omega_A & R_2^A+k_{AB} & -\omega_1 & 0 & -k_{BA} & 0 & 0 & 0 & 0 & 0 & 0 & 0 \\
-2R_1^A p_A & 0 & \omega_1 & R_1^A+k_{AB} & 0 & 0 & -k_{BA} & 0 & 0 & 0 & 0 & 0 & 0 \\
0 & -k_{AB} & 0 & 0 & R_2^B+k_{BA}+k_{BC} & \omega_B & 0 & -k_{CB} & 0 & 0 & 0 & 0 & 0 \\
0 & 0 & -k_{AB} & 0 & -\omega_B & R_2^B+k_{BA}+k_{BC} & -\omega_1 & 0 & -k_{CB} & 0 & 0 & 0 & 0 \\
-2R_1^B p_B & 0 & 0 & -k_{AB} & 0 & \omega_1 & R_1^B+k_{BA}+k_{BC} & 0 & 0 & -k_{CB} & 0 & 0 & 0 \\
0 & 0 & 0 & 0 & -k_{BC} & 0 & 0 & R_2^C+k_{CB}+k_{CD} & \omega_C & 0 & -k_{DC} & 0 & 0 \\
0 & 0 & 0 & 0 & 0 & -k_{BC} & 0 & -\omega_C & R_2^C+k_{CB}+k_{CD} & -\omega_1 & 0 & -k_{DC} & 0 \\
-2R_1^C p_C & 0 & 0 & 0 & 0 & 0 & -k_{BC} & 0 & \omega_1 & R_1^C+k_{CB}+k_{CD} & 0 & 0 & -k_{DC} \\
0 & 0 & 0 & 0 & 0 & 0 & 0 & -k_{CD} & 0 & 0 & R_2^D+k_{DC} & \omega_D & 0 \\
0 & 0 & 0 & 0 & 0 & 0 & 0 & 0 & -k_{CD} & 0 & -\omega_D & R_2^D+k_{DC} & -\omega_1 \\
-2R_1^D p_D & 0 & 0 & 0 & 0 & 0 & 0 & 0 & 0 & -k_{CD} & 0 & \omega_1 & R_1^D+k_{DC}
\end{bmatrix}
\begin{bmatrix}
E/2 \\ I_x^A \\ I_y^A \\ I_z^A \\ I_x^B \\ I_y^B \\ I_z^B \\ I_x^C \\ I_y^C \\ I_z^C \\ I_x^D \\ I_y^D \\ I_z^D
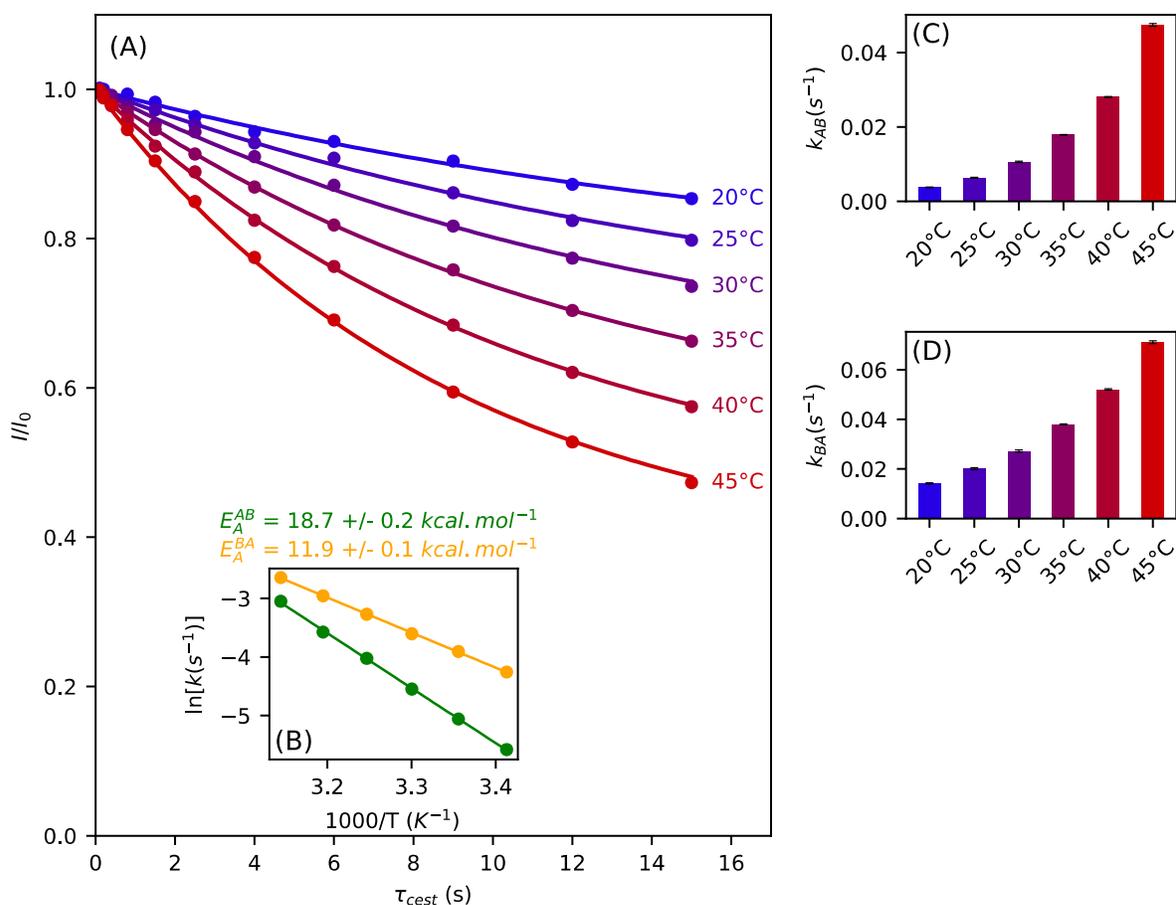\end{bmatrix}
$$

(S5)

Figure S1. CEST characterization of gem-diol (State A) - aldehyde (State B) exchange of DOPAL. (A) Saturation profiles (I/I_0) of the aldehyde as a function of gem-diol saturation time (τ_{cest}) at different temperatures, recorded for a sample containing 2mM DOPAL dissolved in 10 mM sodium phosphate D_2O buffer, pD 7.9. Measurements were carried out at 600 MHz, using a B_1 field of 10 Hz, an interscan delay of 60 s and averaged over 8 transients. Solid lines represent the best fit to the two-state Bloch-McConnell equations described above where the longitudinal and transverse relaxation times are assumed identical for both states ($T_1 = 25$ s, $T_2 = 1$ s). In this particular case, as both states are directly observables in the 1D spectrum, the populations (see Figure S2) and chemical shifts are fixed and only the exchange rate (k_{ex}) is optimized at each temperature. (B) Arrhenius activation energies of this exchange system derived from the fitted k_{ex} values. (C-D) Forward $k_{AB}= (1-p_A)k_{ex}$ and reverse rates, $k_{BA}= p_A k_{ex}$, as a function of temperature.
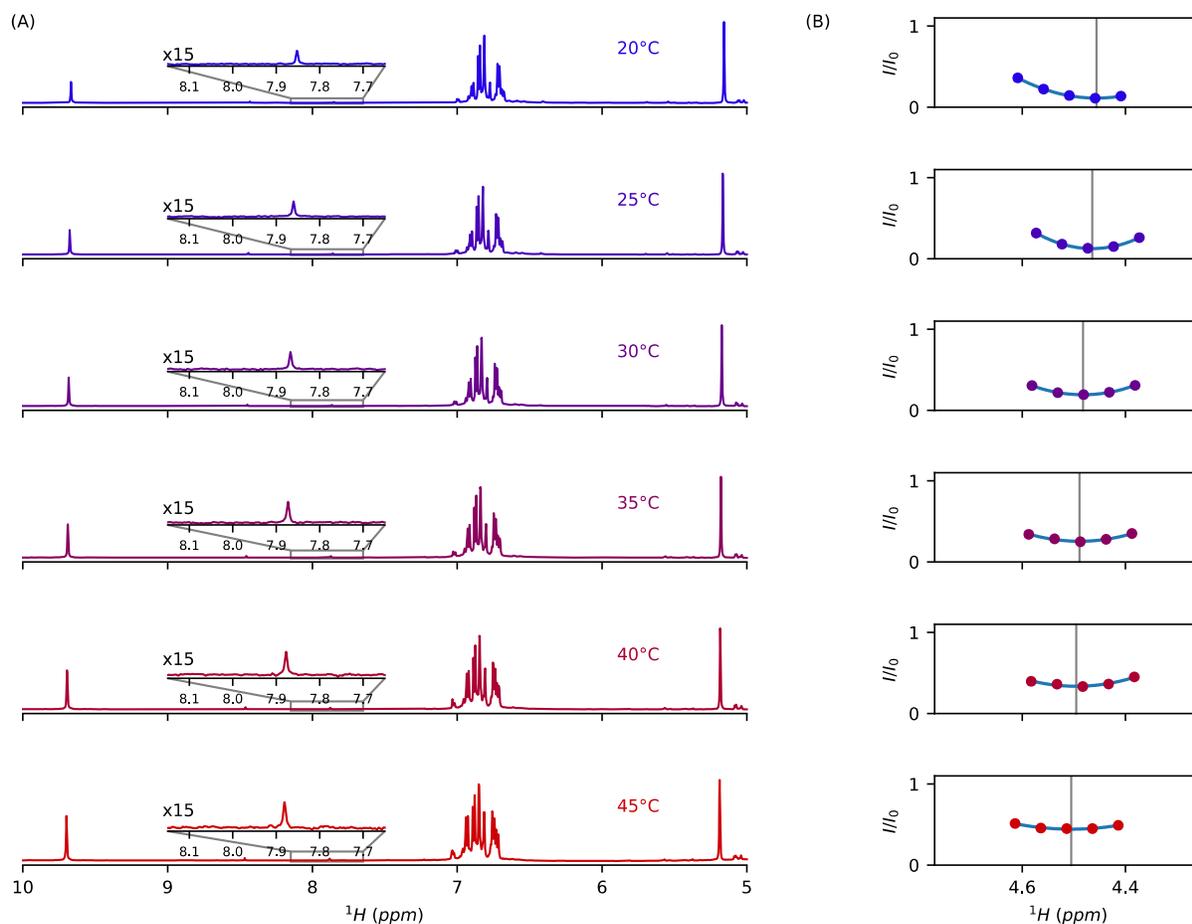
Figure S2. Determination of chemical shifts for Schiff base and its hydrated form in the DOPAL/A$_2$ equilibrium. (A) ^{1}H spectrum used to determine the resonance frequency of the Schiff base measured at 600 MHz with d_1 = 60 s, ns = 64, where d_1 is the interscan delay, and ns is the number of scans. (B) ^{1}H-CEST profile as a function of irradiation frequency, measured at 600 MHz with B_1 = 30 Hz, τ_{cest} = 5 s, d_1 = 60 s and ns = 4. The blue line represents the best fit to a 2nd order polynomial function used to determine the chemical shift of the hydrated Schiff base with δ^{HSB} corresponding to the minimum of this function. Note that the temperature dependence of its chemical shift is opposite to that of HDO, and its amplitude is independent of the residual fraction of HDO in the sample. Experimental data were recorded on a sample containing 2 mM DOPAL and 10 mM A$_2$ dissolved in 10 mM sodium phosphate D$_2$O buffer, pD 7.9.
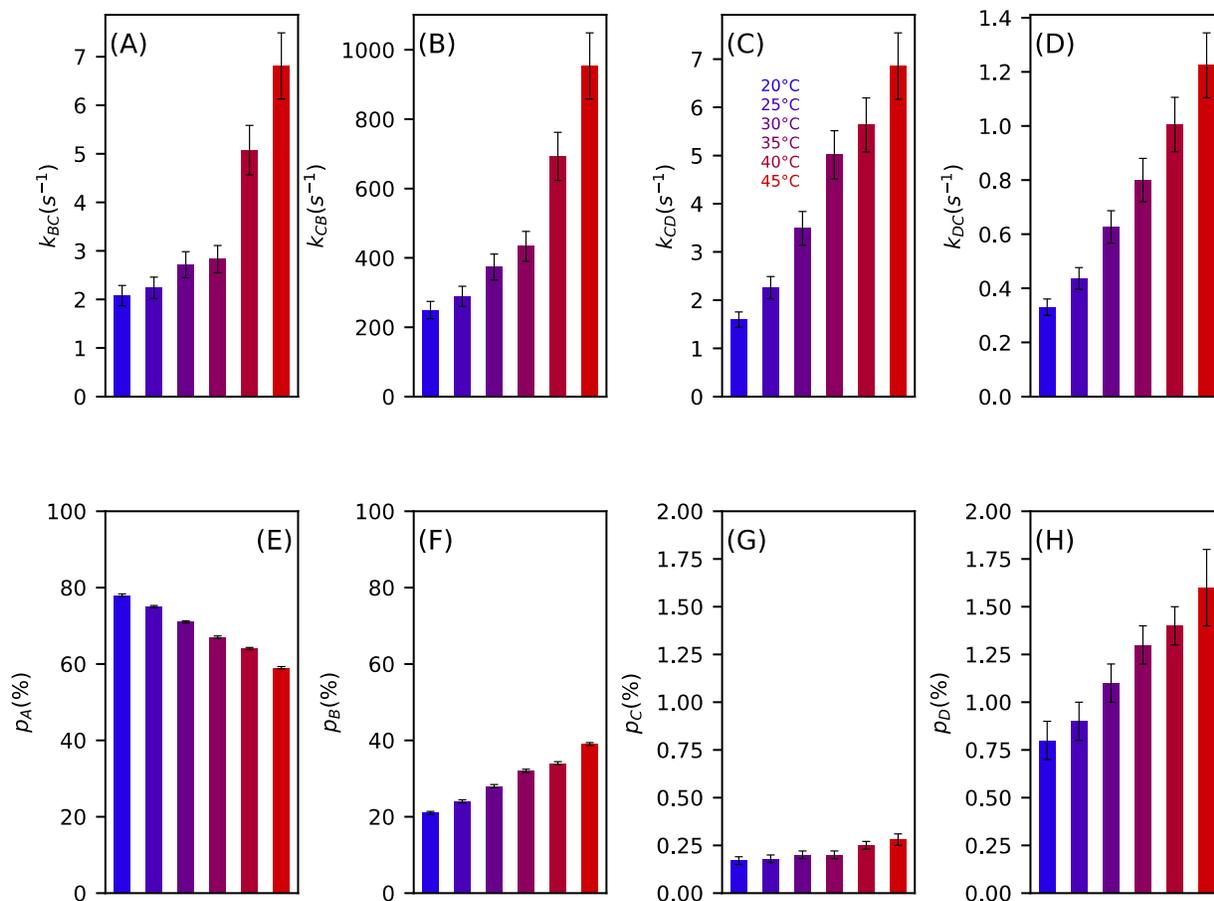
Figure S3. Rates and populations for the DOPAL-A$_2$ equilibrium. (A-D) Exchange rates. (E-H) Populations of each state. Direct observation of the Schiff base resonance allows fitting to be restricted to k_{BC}, k_{CB}, k_{CD}. The value of k_{DC} then follows from the ratio p_B/p_D. Experimental data were recorded on a sample containing 2 mM of DOPAL and 10 mM of A$_2$ prepared by dissolving them in 10 mM de-oxygenated sodium phosphate D$_2$O buffer, pD 7.9.
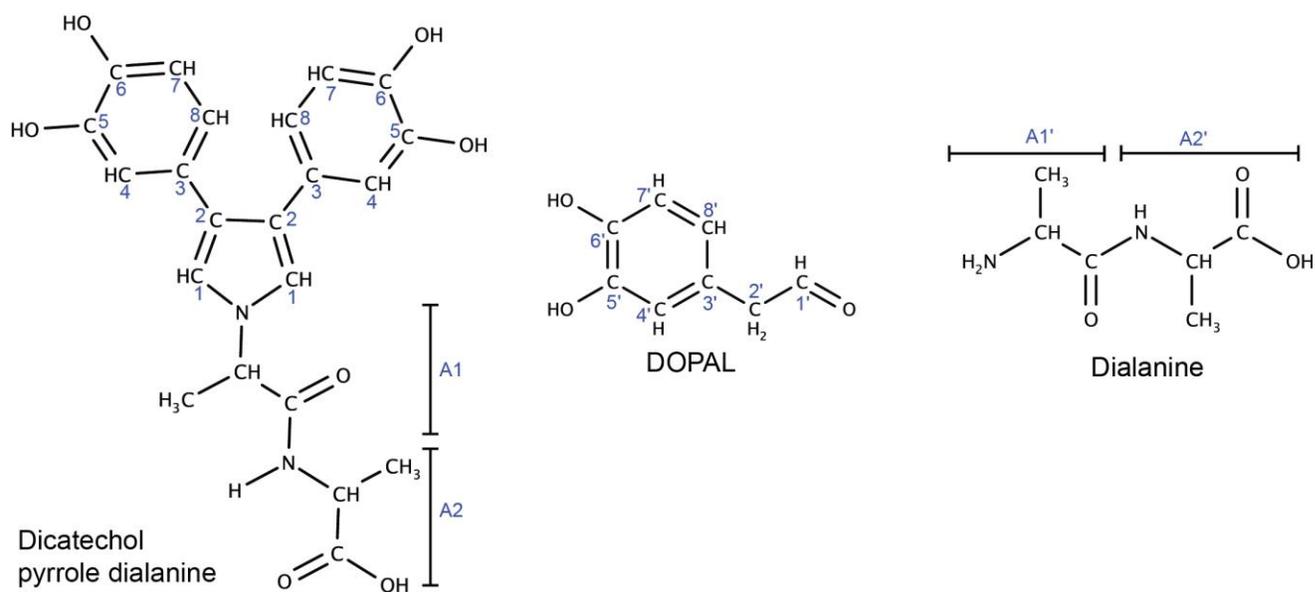
Figure S4. Annotated structures of dicatechol pyrrole di-alanine and the two reactants, DOPAL and di-alanine.
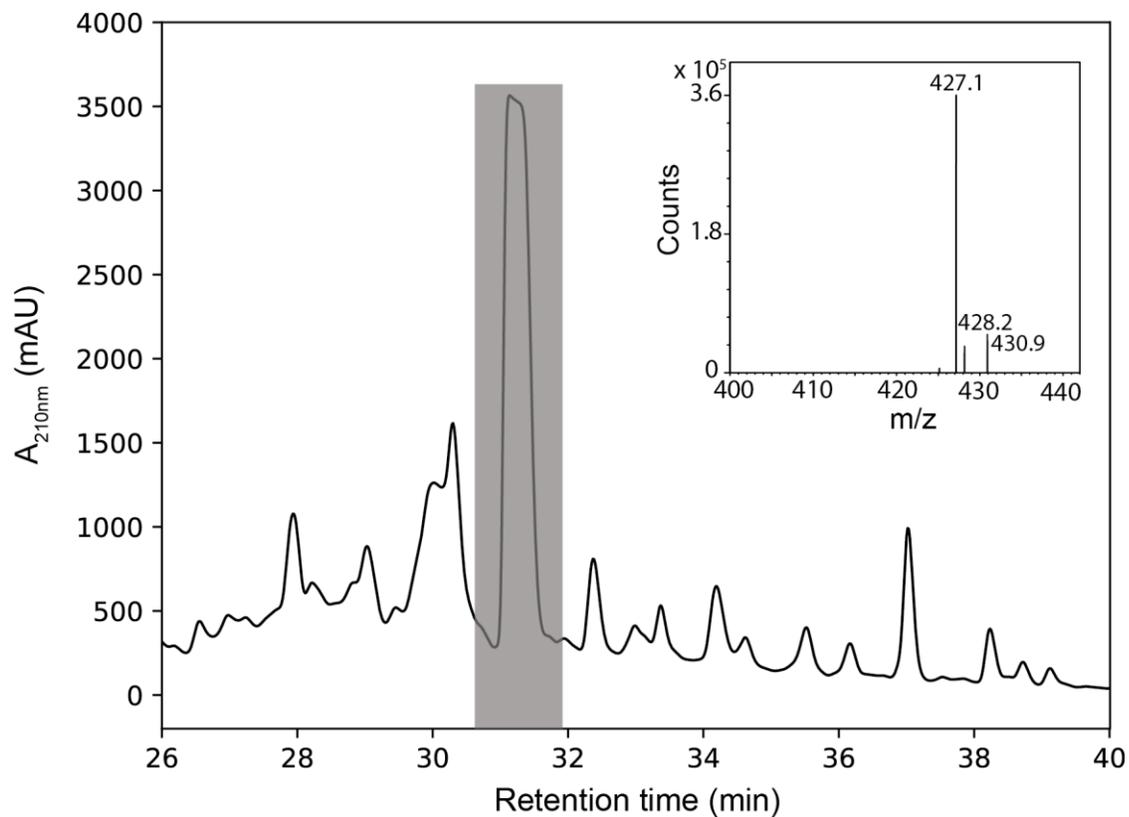
<u>Figure S5.</u> Purification of dicatechol adduct from the reaction between DOPAL and dialanine. HPLC trace from the reaction mixture illustrates the elution of DCPdA at 31 min retention time. The inset shows the deconvoluted mass spectrum of material purified from the shaded region of the HPLC chromatogram, which falls within experimental uncertainty of the expected mass of 426.4 Da.

Figure S6. Full 2D ^{1}H-^{13}C spectra for purified Dicatechol pyrrole dialanine. (A-C) ^{1}H-^{13}C HSQC spectra for the aromatic (A) and aliphatic (B) resonances, (C) the ^{1}H-^{13}C HMBC spectrum are shown with signal labels corresponding to the numbering of Figure S4.

Figure S7. Saturation profiles of the aldehyde resonance in the presence AcL upon irradiation of (A-C) the hydrated and (D-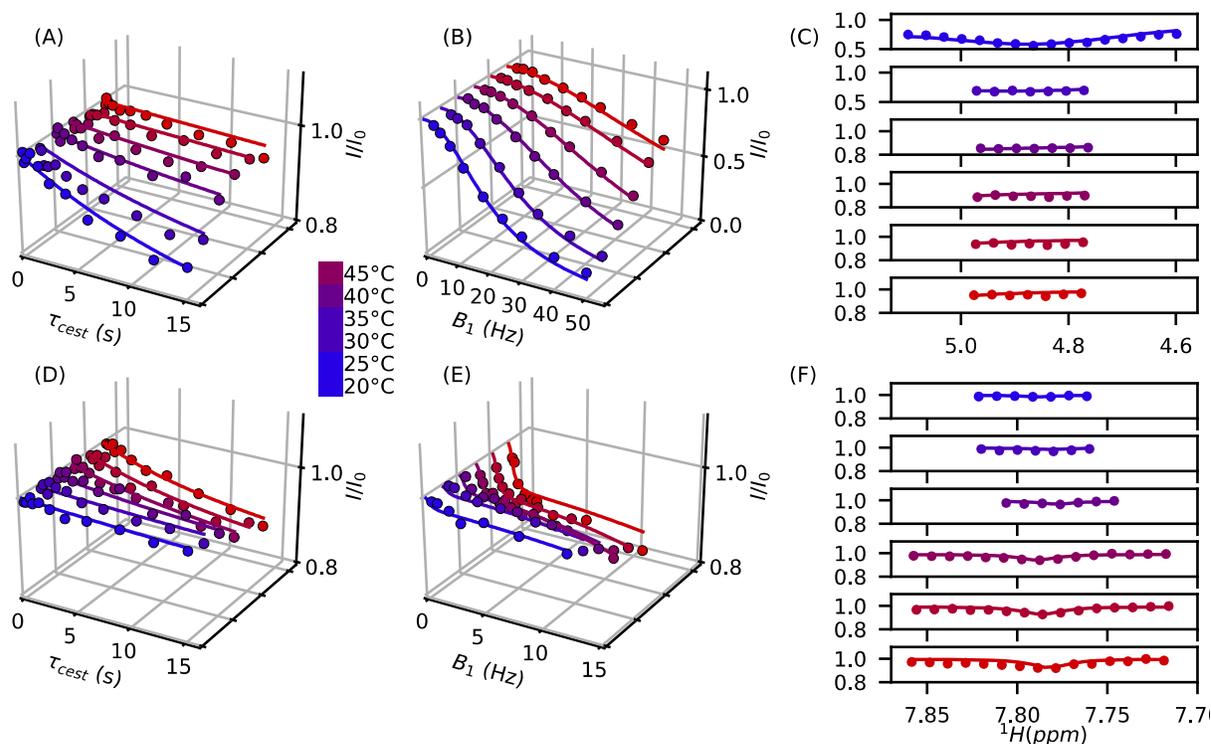F) dehydrated Schiff base resonance for temperatures ranging from 20 ºC to 45 ºC. (A) On-resonance saturation recorded with $B_1 = 10$ Hz and τ_{cest} ranging from 0.1 to 15 s. (B) Saturation recorded with $\tau_{cest} = 30$ s and B_1 ranging from 3 to 50 Hz. (C) Aldehyde attenuation profile recorded with $B_1 = 30$ Hz and $\tau_{cest} = 5$ s as a function of irradiation frequency. (D) Saturation recorded with $B_1 = 5$ Hz and τ_{cest} ranging from 0.1 to 15 s. (E) Saturation recorded with $\tau_{cest} = 30$ s and B_1 ranging from 0.5 to 12 Hz. (F) Aldehyde attenuation profile as a function of irradiation frequency recorded with $B_1 = 6$ Hz and $\tau_{cest} = 15$ s. Rate constants fitted to these profiles as well as populations of HSB$_{AcL}$ (p_C) and DSB$_{AcL}$ (p_D) as a function of temperature are shown in Figure 3 of the main text. Data were recorded on a sample containing 2 mM DOPAL and 30 mM AcL in 10 mM sodium phosphate D_2O buffer, pD 7.9.
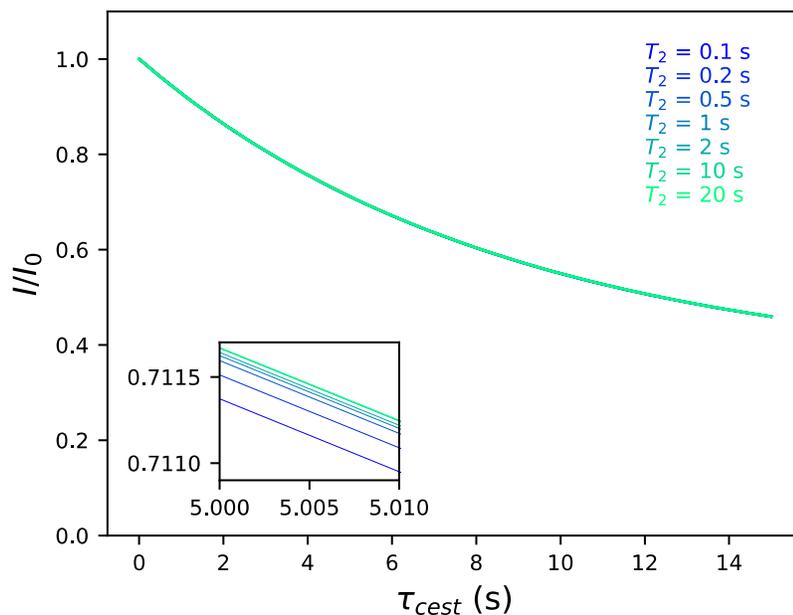
Figure S8. Effect of the transverse relation rate (R_2) on saturation profiles simulated for a two-state exchanging system with $B_0 = 600$ MHz, $B_1 = 10$ Hz, $T_{1,A} = T_{1,B} = 25$ s, $\delta_A = 5.1$ ppm, $\delta_B = 9.609$ ppm, $p_A = 0.79$, $\omega_{rf} = 5.1$ ppm, $k_{ex} = 0.1$ Hz.

Figure S9. Superimposed zoomed region of the ^{1}H NMR spectra of 2mM DOPAL in the absence (red) and presence (blue) of 10 mM A$_2$ measured at 600 MHz in 10 mM sodium phosphate D$_2$O buffer, pD 7.9, and T = 35ºC.

Table S1. Summary of NMR data for Dicatechol pyrrole dialanine product and two reactants, DOPAL and dialanine

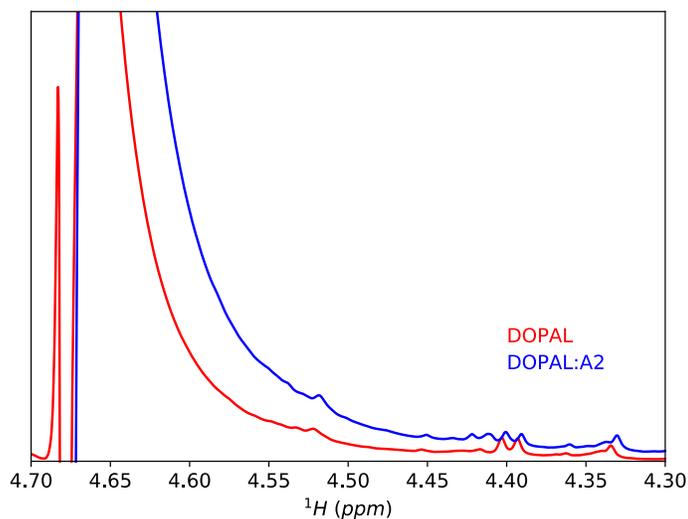| Dicatechol pyrrole dialanine			DOPAL			Dialanine		
	^{1}H (ppm)	^{13}C (ppm)		^{1}H (ppm)	^{13}C (ppm)		^{1}H (ppm)	^{13}C (ppm)
A2-C'		177.311				A2'-C'		178.684
A1-C'		172.801				A1'-C'		169.841
A2-C$^\alpha$	4.304	50.652				A2'-C$^\alpha$	3.905	51.483
A2-C$^\beta$	1.365	18.347				A2'-C$^\beta$	1.379	18.871
A1-C$^\alpha$	4.778	58.788				A1'-C$^\alpha$	4.238	50.244
A1-C$^\beta$	1.697	18.277				A1'-C$^\beta$	1.509	17.422
1	6.798	119.217	1'	4.582	100.673			
2		124.817	2'	2.650, 2.726	43.790			
3		129.537	3'		130.080			
4	6.688	116.797	4'	6.680	117.660			
5		145.557	5'		145.842			
6		144.207	6'		144.650			
7	6.641	115.957	7'	6.657	115.962			
8	6.581	120.957	8'	6.535	121.770			

Table S2. Summary of rates and populations for each equilibrium

	20ºC	25ºC	30ºC	35ºC	40ºC	45ºC
gem-diol / aldehyde equilibrium						
$p_{aldehyde}$ (%)	21.1 ± 0.2	24.1 ± 0.2	28.1 ± 0.2	32.1 ± 0.2	34.9 ± 0.2	39.9 ± 0.3
$P_{gem\text{-}diol}$ (%)	78.9 ± 0.2	75.9 ± 0.2	71.9 ± 0.2	67.9 ± 0.2	65.1 ± 0.2	60.1 ± 0.3
k_{AB} (s^{-1})	0.004 ± 0.001	0.006 ± 0.001	0.01 ± 0.002	0.02 ± 0.002	0.03 ± 0.003	0.05 ± 0.004
k_{BA} (s^{-1})	0.01 ± 0.003	0.02 ± 0.004	0.03 ± 0.004	0.04 ± 0.004	0.05 ± 0.005	0.07 ± 0.006
DOPAL-A$_2$ equilibrium						
k_{BC} (s^{-1})	2.1 ± 0.2	2.2 ± 0.2	2.7 ± 0.3	2.8 ± 0.3	5 ± 0.5	6.8 ± 0.7
k_{CB} (s^{-1})	249 ± 25	289 ± 29	373 ± 37	433 ± 43	693 ± 70	953 ± 95
k_{CD} (s^{-1})	1.6 ± 0.2	2.3 ± 0.2	3.5 ± 0.4	5.0 ± 0.5	5.6 ± 0.6	6.9 ± 0.7
k_{CD} (s^{-1})	0.3 ± 0.03	0.4 ± 0.04	0.6 ± 0.06	0.8 ± 0.08	1.0 ± 0.1	1.2 ± 0.1
p_A (%)	78.7 ± 0.3	75.7 ± 0.3	$71..7 \pm 0.3$	67.7 ± 0.3	64.6 ± 0.3	59.6 ± 0.3
p_B (%)	20.1 ± 0.3	23.1 ± 0.3	27.2 ± 0.3	31.0 ± 0.3	33.8 ± 0.3	38.8 ± 0.4
p_C (%)	0.17 ± 0.02	0.18 ± 0.02	0.20 ± 0.02	0.20 ± 0.02	0.25 ± 0.02	0.28 ± 0.03
p_D (%)	0.88 ± 0.1	0.98 ± 0.1	1.12 ± 0.1	1.31 ± 0.1	1.32 ± 0.1	1.48 ± 0.1
DOPAL-AcL equilibrium						
k_{BC} (s^{-1})	2.5 ± 0.3	5.9 ± 0.6	9.8 ± 1	19.8 ± 2	31.4 ± 3	38.4 ± 4
k_{CB} (s^{-1})	818 ± 82	1523 ± 150	3163 ± 320	6095 ± 610	13481 ± 1350	24130 ± 2400
k_{CD} (s^{-1})	0.5 ± 0.05	0.4 ± 0.04	0.9 ± 0.1	1.8 ± 0.2	3.6 ± 0.4	6.3 ± 0.6
k_{DC} (s^{-1})	2.0 ± 0.2	2.0 ± 0.2	2.2 ± 0.2	2.0 ± 0.2	1.9 ± 0.2	2.0 ± 0.2
p_A (%)	78.9 ± 0.3	75.9 ± 0.3	71.9 ± 0.3	67.9 ± 0.3	65.0 ± 0.3	60.0 ± 0.3
p_B (%)	21.0 ± 0.3	24.0 ± 0.3	28.0 ± 0.3	31.9 ± 0.3	34.8 ± 0.3	39.7 ± 0.3
p_C (%)	0.06 ± 0.006	0.09 ± 0.01	0.09 ± 0.01	0.1 ± 0.01	0.08 ± 0.01	0.07 ± 0.02
p_D (%)	0.014 ± 0.01	0.015 ± 0.002	0.034 ± 0.003	0.093 ± 0.01	0.16 ± 0.002	0.21 ± 0.02

References

[1] F. Delaglio, S. Grzesiek, G. W. Vuister, G. Zhu, J. Pfeifer, A. Bax, *J. Biomol. NMR* **1995**, *6*, 277-293.

[2] J. J. Helmus, C. P. Jaroniec, *J. Biomol. NMR* **2013**, *55*, 355-367.

[3] B. Efron, R. J. Tibshirani, *An Introduction to the Bootstrap*, Chapman & Hall, Washington DC, **1993**.

[4] P. Vallurupalli, G. Bouvignies, L. E. Kay, *J. Am. Chem. Soc.* **2012**, *134*, 8148-8161.